

Molecular Dynamics Study of Surfactant-Like Peptide Based Nanostructures

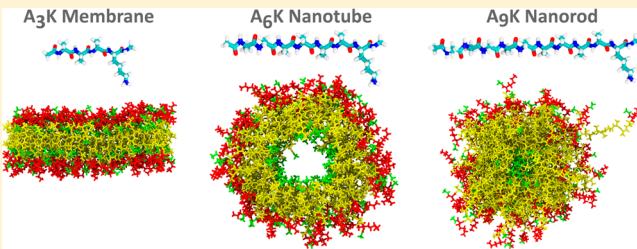
Guilherme Colherinhas[†] and Eudes Fileti*,‡

[†]Departamento de Física, CEPAE, Universidade Federal de Goiás, CP. 131, 74001-970, Goiânia, GO, Brazil

[‡]Instituto de Ciência e Tecnologia, Universidade Federal de São Paulo, 12231-280, São José dos Campos, SP, Brazil

S Supporting Information

ABSTRACT: Surfactant-like peptide (SLP) based nanostructures are investigated using all-atomistic molecular dynamics (MD) simulations. We report structure properties of nanostructures belonging to the A_NK peptide group. In particular, the mathematical models for the two A₃K membranes, A₆K nanotube, and A₉K nanorod were developed. Our MD simulation results are consistent with the experimental data, indicating that A₃K membranes are stable in two different configurations: (1) SLPs are tilted relative to the normal membrane plane; (2) SLPs are interdigitated. The former configuration is energetically more stable. The cylindrical nanostructures feature a certain order of the A₆K peptides. In turn, the A₉K nanorod does not exhibit any long-range ordering. Both nanotube and nanorod structure contain large amounts of water inside. Consequently, these nanostructures behave similar to hydrogels. This property may be important in the context of biotechnology. Binding energy analysis—in terms of Coulomb and van der Waals contributions—unveils an increase as the peptide size increases. The electrostatic interaction constitutes 70–75% of the noncovalent attraction energy between SLPs. The nanotubular structures are notably stable, confirming that A₆K peptides preferentially form nanotubes and A₉K peptides preferentially form nanorods.



1. INTRODUCTION

The peptide based materials are in the focus of vigorous research within recent years due to their versatility, biocompatibility, and fascinating medicinal properties.^{1–11} The manifold applications of artificial self-assembling nanostructures in biotechnology and biomedicine are continuously pursued.^{2,3,7,8,12–14} The self-assembled peptides inspired numerous research efforts to shape novel developments and engineering setups. For instance, the field of regenerative medicine has evolved very rapidly. This field may bring a groundbreaking progress in the treatment of heart failure and diabetes.⁷ Furthermore, the properties of peptides, such as their natural antimicrobial activity, are interesting in medicine. Antimicrobial action of various peptides was extensively attended over the last two decades.^{15–24} The antimicrobial peptides are considered to exhibit selectivity for bacterial membranes, a broad spectrum of antibacterial and antifungal activity, and antiviral and anticancer activity.^{24–28} The clinical trials of some formulations have already been performed.²⁹

An important class of peptides with antimicrobial action is peptide amphiphiles.^{4,6,7,11,21,30,31} By structure, these molecules resemble lipids or detergents. They are equipped with a hydrophilic headgroup and a hydrophobic tail. Consequently, self-assembly of peptide amphiphiles is possible in aqueous environments.¹² The spatial arrangement in the self-assembled structure is affected by (1) peptide conformation, (2) physicochemical properties of the environment (pH, temperature, ionic strength), (3) concentration of amphiphiles, and

partially (4) initial system configuration. A variety of supramolecular morphologies—fibrils, nanorods, nanotubes, bilayers—may be obtained in such a way.^{32,33}

The relationship between the antibacterial activity of surfactant like peptides (SLPs) and their nanostructure formation ability was investigated experimentally. Zhao et al. examined this relationship for the A_NK peptide.^{34,35} They synthesized three different peptide structures with N = 3, 6, and 9, observed the formation of nanostructures, and characterized an antibacterial activity. The A₃K, A₆K, and A₉K peptides were self-organized in bilayers, nanotubes, and nanorods, respectively.³⁵ A₃K clearly exhibits a low antibacterial activity, while A₆K exhibits a moderate activity.²¹ A₉K is the most efficient based on the biological experiments, which confirmed the death of bacteria. It was hypothesized that the antimicrobial action takes place due to the mechanistic rupture of the bacterial membrane by a longer oligopeptide (A₉K).²¹

This work reports an extensive molecular dynamics (MD) study, with an atomistic resolution, to describe the structure and energetics of the self-assembled nanostructures of A₃K, A₆K, and A₉K amphiphilic peptides. Description of these structures at the molecular level and understanding of their intermolecular interactions are important steps to understand

Received: August 15, 2014

Revised: September 27, 2014

Published: September 29, 2014

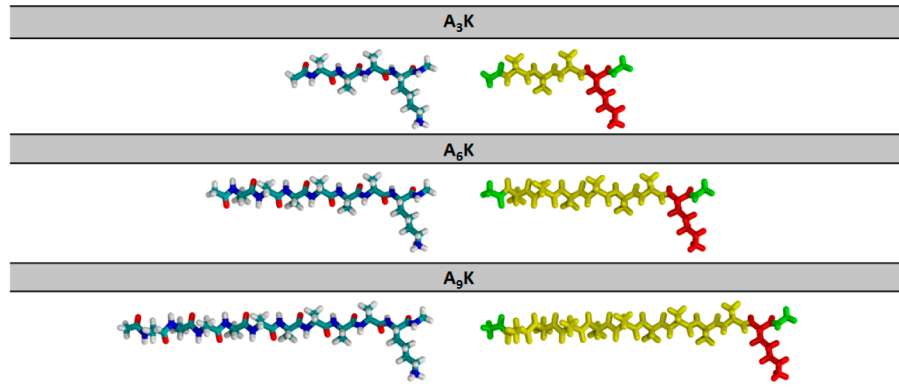


Figure 1. A_{NK} ($N = 3, 6$, and 9) peptides that form the structures investigated in this work. This group includes one hydrophobic tail (A, alanine, in yellow) and a charged hydrophilic head lysine (K, lysine, in red). Acetylated (CH_3CO^-) and amidated (CH_3NH^-) termini are shown in green.

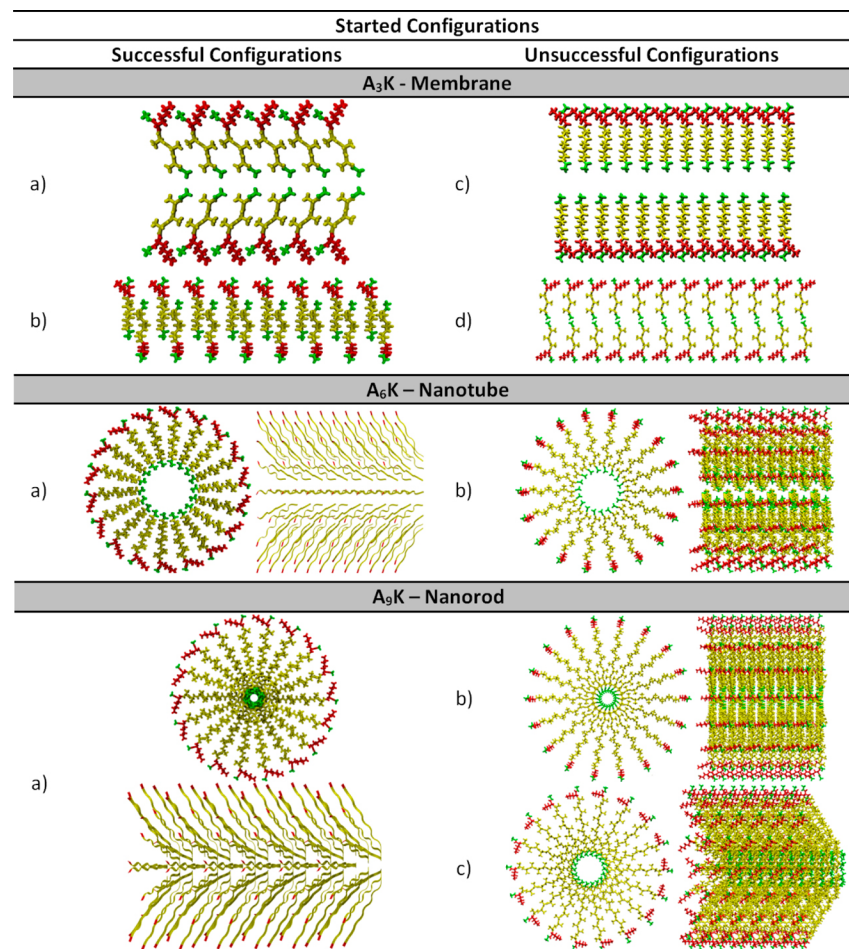


Figure 2. (left) A_{NK} successful starting structures and (right) some A_{NK} unsuccessful tested starting structures.

how the hydrophobic tail length modulates the self-assembly thermodynamics and kinetics.

2. METHODS

2.1. Simulated Systems. The nanostructures investigated in this work are composed by the A_{NK} peptides. These peptides are, in turn, composed by three, six, and nine alanine residues (hydrophobic moiety) and a charged lysine headgroup (hydrophilic moiety). The schematic representation is given in Figure 1. Each system was initially preassembled using juxtaposition of smaller polypeptides, such as dimers or rings.

The major purpose of this initial arrangement is to foster formation of the intermolecular hydrogen bonds. The presence of hydrogen bonds was experimentally suggested previously.³⁵ The schematic representation of all successful and some unsuccessful initial configurations is given in Figure 2. The geometric details of these configurations are described in the Supporting Information. As soon as the hydrogen bonding network is established, self-assembly proceeds quickly. Chloride anions were added to neutralize all systems. The input geometry of the system was optimized in a vacuum using pairwise interaction potentials (CHARMM36 force field).

Finally, the amphiphiles were hydrated. The compositions of all the simulated systems are provided in Table 1.

Table 1. Composition of All Successful Nanostructures^a

system	type	# A _N K (atom per A _N K)	# ions	# water molecules	total number of atoms
A ₃ K _C	tilted membrane	144 (64)	144	3863	20949
A ₃ K _T	intercalated membrane	128 (64)	128	3322	18286
A ₆ K	nanotube	108 (94)	108	11736	45468
A ₉ K	nanorod	108 (124)	108	18534	69102

^aThe number in parentheses refers to the number of interaction centers (atoms) in each A_NK peptide. The total number of atoms in the last column includes all ions in the systems, which were necessary to compensate the net charge of the nanostructure.

2.2. Simulation Details. Hydrated nanostructures were simulated according to our recent protocol.² The CHARMM36 force field³⁶ was employed to describe bonded and nonbonded molecular interactions in the system. The MD cells were equilibrated for 10 ns. The production stage was performed for 100 ns. All MD simulations were performed in the constant temperature constant pressure ensemble (N, P, T). The equations of motion were integrated using a time step of 2.0 fs. Such a relatively large time step was possible by constraining all covalent bonds exhibiting high oscillation frequencies. The trajectory frames were recorded every 20 ps and consisted exclusively of atom positions. The MD systems were maintained at constant temperature (300 K) using the velocity

rescaling thermostat with a coupling constant of 0.1 ps. The constant external pressure was maintained using the semi-isotropic implementation of the Parrinello–Rahman barostat,³⁷ with a relaxation time of 2.0 ps. All bond lengths were constrained using the LINCS algorithm.³⁸ That is, the conformation flexibility of oligopeptides was reproduced by harmonic angle potentials. A cutoff distance of 1.2 nm for LJ interaction was employed. The Coulomb interactions beyond the real-space cutoff of 1.2 nm were treated using the particle-mesh Ewald technique,³⁹ in accordance with the CHARMM36 specifications. All MD simulations were performed in the GROMACS 4.6.5 program suite.^{40,41} Image rendering and visual analysis were performed in the Visual Molecular Dynamics (VMD) program.⁴²

3. RESULTS AND DISCUSSION

The stabilization of the SLP based nanostructures is different from the mechanism reported for lipopeptides.^{11,43,44} The lipopeptides are equipped with a large hydrophobic tail, which is responsible for the formation of the core (Figure 1). In the case of SLPs, the hydrophobic tail is mimicked by a specific sequence of the hydrophobic amino acid residues. However, the hydrophobicity of these amino acid residues is significantly different as compared to polypeptides. In addition, –CO and –NH groups interact electrostatically. As we illustrated previously,² the nanostructure is stabilized by the two interaction types: (1) weak hydrophobic attraction between the amino acid residues and (2) stronger electrostatically driven attraction between peptide bridges (–CO…HN–).² The membrane surface consists of hydrophilic charged groups exposed to an aqueous environment. The polar groups can be

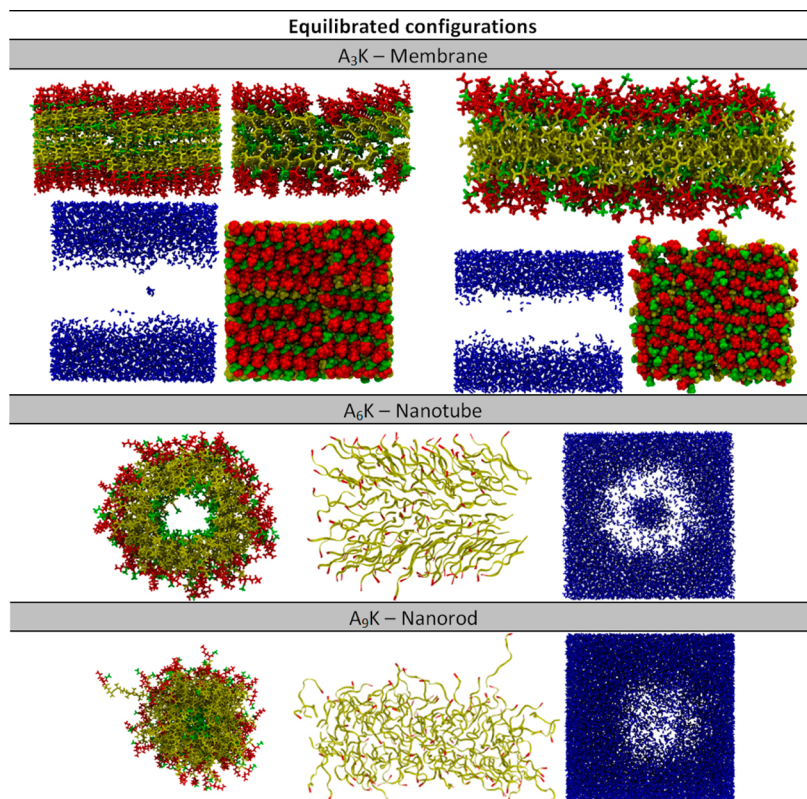


Figure 3. Representation of the lateral and frontal views for the A₃K membranes, A₆K nanotube, and A₉K nanorod (with water omitted). In blue, the views of the water molecule distribution (with SLP omitted) are presented.

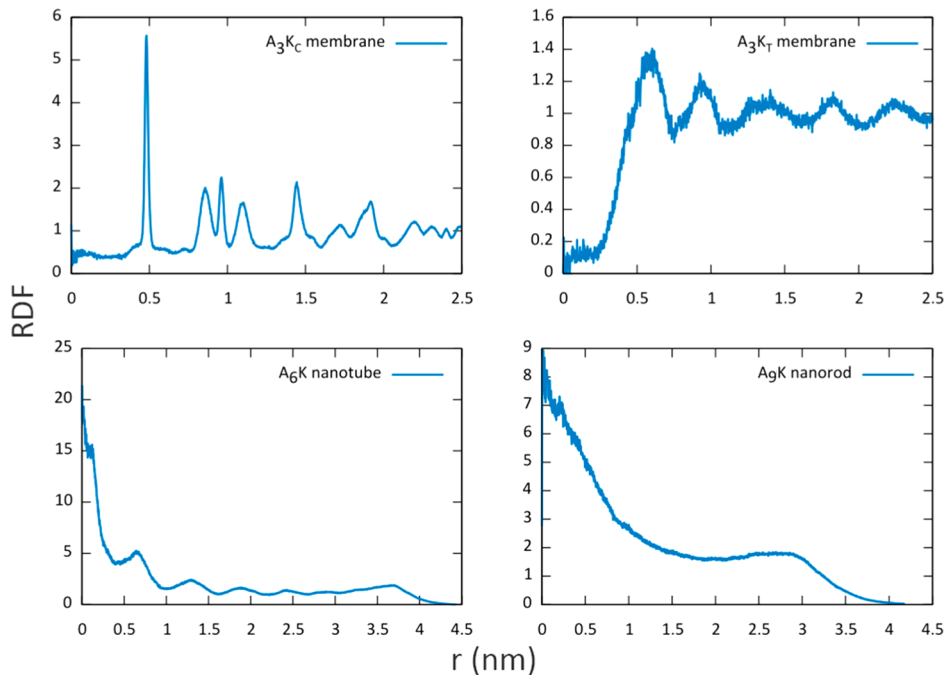


Figure 4. Planar radial distribution functions (RDFs) calculated for the center of mass of the SLP backbone.

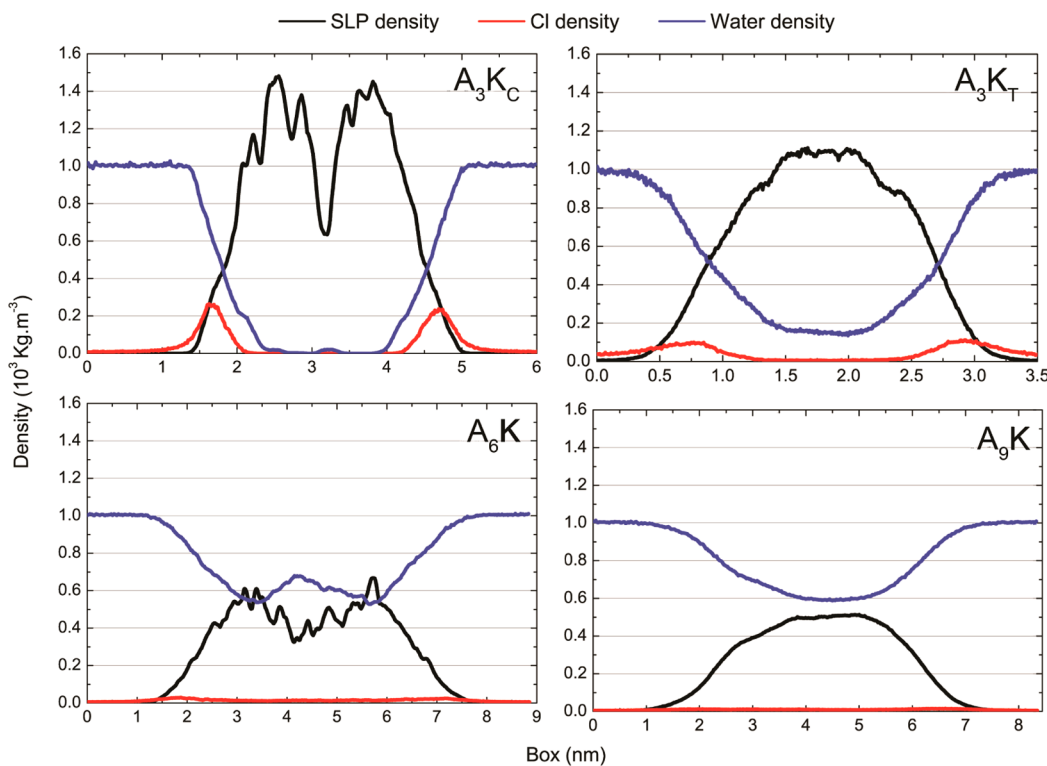


Figure 5. Mass density distribution for (top) A_3K membranes calculated along the membrane normal direction and for (bottom) A_6K and A_9K systems calculated along the lateral plane.

both positively and negatively charged as a whole. In comparison, conventional lipid membranes are stabilized by lateral forces keeping polar groups together in the proximity of hydrophilic media. The latter arrangement results in a looser membrane and vesicle structures.²

A_NK -type peptides are composed of a polar group attached to hydrophobic residues. In the present case, alanine residues were employed. The number of residues determines, in essence,

the type of the self-assembled nanostructure. According to recent research, the particular self-assembled structure plays the most important role in the antimicrobial activity.²¹ Self-assembly can be easily implemented in direct *in vitro* experiments.³ However, the nonequilibrium computer simulations of self-assembly are not straightforward. It is because of a very complicated free energy landscape and due to the limited amount of the explicitly simulated water. For instance, the

initial structures based on the stacked monolayers and flat rings of SLP (Figure 2) were not stable during spontaneous MD. The two stable configurations were found in the case of A₃K membranes. The first configuration, A₃K_C, involves SLPs tilted with respect to the membrane normal plane. The second configuration, A₃K_T, involves interdigitated SLPs. Both A₆K nanotubes and A₉K nanorods are stable nanostructures. Figure 3 summarizes only equilibrated configurations.

Planar radial distributions of the centers of mass of the A_NK peptide are depicted in Figure 4. These distributions provide a description of the membrane in terms of the probability to find A_NK's neighbors close to a reference SLP molecule. Both A₃K membranes exhibit an ordered structure over long distances. The A₃K_C containing membrane exhibits a solid-like structure, based on the repetitive RDF peaks (Figure 4). In the case of a nanotube and a nanorod, a strong peak is present at the center and decays gradually. However, undulations in the spatial distributions of A₆K peptides indicate that a nanotube conformation exhibits a certain structure order. In turn, A₉K exhibits no order (uniformly decreasing RDF). The described structure patterns can be directly observed in the equilibrated structures (Figure 3).

The interface formed by a nanostructure and water is analyzed in terms of mass density profiles (Figure 5). In all systems, one observes a diffuse interfacial behavior of the mass densities, which prevents from a clear distinguishing between the aqueous phase and the nanostructure. A significant volume of water is found inside all nanostructures. In fact, a large amount of water is found inside all nanostructures, with the exception of A₃K_C membrane, for which only the surface contact (with small water penetration) was observed. On the other hand, nearly a half of the A₆K nanotube and the A₉K nanorod is occupied by water, volumetrically. This is a remarkable feature, indicating that these nanostructures behave like hydrogels. The hydrogels are capable of retaining large amounts of water inside and are, therefore, deemed to foster various applications in biotechnology.⁴⁵

A certain amount of water is observed at the center of the A₆K nanotube. All water molecules have quickly penetrated between the peptides during spontaneous MD simulations, while they were deliberately removed at the beginning of the simulation. The primary reason for such a hydration type is relatively strong attraction between alanine residues and water molecules. Compare with the conventional lipid bilayers, where the core is notably hydrophobic. The additional trials have been performed with the smaller-diameter nanotubes to avoid encapsulated water molecules. However, these self-assembled configurations are less thermodynamically stable.

The membrane thickness and diameters (in the case of cylindrical nanostructures, A₆K and A₉K) are readily extractable from mass density distributions (Table 2). Compared with lipids, these membranes are very thin, 2.6 nm (A₃K_C) and 1.9 nm (A₃K_T). The A₃K_C model is consistent with the results of Xu et al.,³⁵ which inferred a bilayer formation by these nanostructures. The AFM phase image suggests structure and mechanical homogeneity of the A₃K membranes. We use a grid-based method (Figure 6) to determine the variations of membrane thickness.⁴⁶ Indeed, all membranes are reasonably homogeneous. The thickness at various points varies by less than 0.7 nm.

The A₆K nanotube exhibits an outer diameter of 4.9 nm and an inner diameter of 1.5 nm. The outer diameter is in an excellent agreement with the experimental value, 5.0 ± 1.0 nm,

Table 2. Properties of the A₃K Membranes, A₆K Nanotube, and A₉K Nanorod^a

membranes	<i>l</i>	<i>A</i>	<i>D_P</i>	<i>D_W</i>
A ₃ K _C	2.6	0.22	0.026	4.07
A ₃ K _T	1.9	0.34	0.007	4.51
nanotube/rod	<i>d</i>	<i>A</i>	<i>D_P</i>	<i>D_W</i>
A ₆ K	4.9	0.16	0.0004	3.37
A ₉ K	4.4	0.14	0.007	3.75

^a *A*, *d*, and *l* stand for area per peptide (in nm²), nanotube and nanorod diameters (in nm), and thickness of the membrane (in nm), respectively. *D_P* and *D_W* are the diffusion coefficients (in nm² s⁻¹) of protein and water, respectively.

obtained from the AFM image.³⁵ For all systems investigated in this work, we perform preliminary tests that allowed us to find a stable starting configuration, consistent with the experimental dimensions. For A3K membranes and A6K nanotubes, configurations were found whose dimensions are in good agreement with the experimental value. However, for the nanorod, among all stable structures, which we could conceive, that is closest to the experimental value (for the radius of 3.7 nm),³⁵ is the one described in Figure 3. In this situation, the nanorod has a diameter of 4.4 nm and their peptides are tilted by 65° relative to the tube axis. However, this value agrees qualitatively well with their corresponding experimental value.

Table 2 summarizes the area per peptide. For membranes, this is a total area of the membrane surface divided by the number of surface forming peptides. In the case of cylindrical nanostructures, the area per lipid corresponds to the area of their cross section. It is calculated by dividing an average diameter by the number of peptides. The peptides in the A₃K_T membrane occupy a significantly larger area, 0.34 nm², than in the A₃K_C membrane, 0.22 nm². One could expect that the first number is twice larger than the second number. POPC and 16SM lipid membranes possess areas per lipid of 0.64 and 0.55 nm², respectively (Table S3, Supporting Information). The area per lipid in the A₆K nanotube is 0.16 nm², whereas the area per lipid in the A₉K nanotube is slightly smaller, 0.14 nm². The linear density (number of peptides per unit length) is equal to 11.4 and 19.5 nm⁻¹ for the A₆K and A₉K structures, respectively. These values are comparable to 19.2 nm⁻¹, obtained by Schatz and co-workers for lipopeptide fibers.⁴⁴

The diffusion coefficient, *D_P* (Table 2), is a measure of the lateral mobility of the peptide. It can be related to the rigidity of the nanostructure. *D_P* is a measure of lipid mobility in the biological membranes. *D_P* ranges from ca. 0.003 to 0.008 nm² s⁻¹ for POPC and SM membranes, respectively.² In the A₃K membranes, the peptides exhibit a somewhat larger mobility, 0.026 nm² s⁻¹. This value is much larger than that for lipids in biological membranes. The A₆K nanotube exhibits the lowest mobility among this kind of structures, ca. 0.0004 nm² s⁻¹. This result is consistent with the expected stiffness increase in this nanostructure.³⁵ In the A₃K_C containing membranes, water diffusion, *D_W*, is similar to self-diffusion of bulk water. However, water diffusion is lower around cylindrical nanostructures. This is due to a large volume of water confined inside the nanostructure, in direct contact with the peptide bonds.

Tables 3 and 4 show the energy analysis to the nanostructures studied here. This analysis, although not including entropic contributions, allows us to quantitatively assess the balance of forces in the systems. Table 3 shows the components of the interaction energy between peptides and

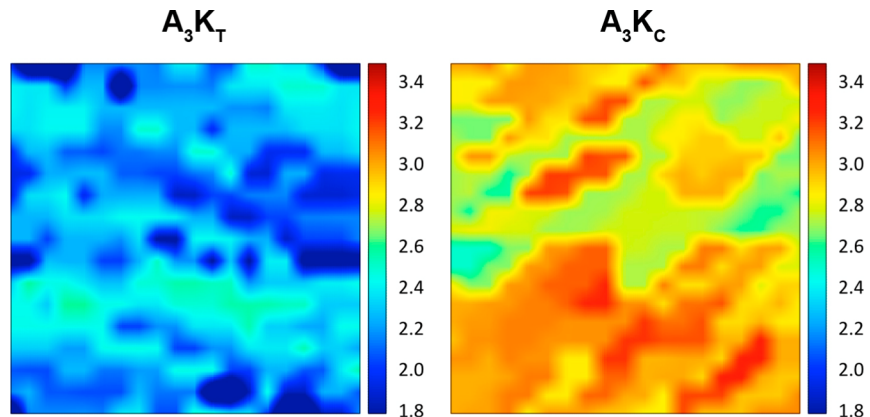


Figure 6. Membrane thickness as a function of two-dimensional position along the SLP bilayer. Color bars represent the thickness from 1.8 nm (blue) to 3.4 nm (red). The thickness was averaged over 25 snapshots (one snapshot every 1 ns) over the final 25 ns of the trajectory.

Table 3. Water–Peptide Interaction Energies (in 10^4 kJ mol $^{-1}$)^a

	U_{Coul}	U_{vdW}	U_{inter}	$\Delta\%$	U_{intra}	U_{total}
Membranes						
A ₃ K _C	-3.2	-0.4	-3.6	11	-17.2	-20.8
A ₃ K _T	-1.7	-0.2	-1.9	8	-22.0	-23.9
Nanotube/Rod						
A ₆ K	-4.4	-0.6	-5.0	12	-47.4	-52.4
A ₉ K	-6.0	-1.0	-7.0	14	-71.8	-78.8

^a U_{Coul} and U_{vdW} are the Coulomb and van der Waals contributions for the intermolecular water–peptide interaction. U_{inter} is the intermolecular energy, obtained by the direct sum of U_{Coul} and U_{vdW} . $\Delta\%$ is the percentage of energy of the intermolecular of van der Waals nature. U_{intra} is the intramolecular energy and U_{total} is the total potential energy of the system obtained by the direct sum of U_{intra} and U_{inter} .

Table 4. Coulomb (U_{Coul}) and van der Waals (U_{vdW}) (in 10^4 kJ mol $^{-1}$) Contributions to Interaction Energy (per Peptide) between the SLPs for Each Nanostructure^a

	U_{Coul}	U_{vdW}	# HBs SS	# HBs AA	# HBs AK
Membranes					
A ₃ K _C	-331	-139	4.7	1.9	1.0
A ₃ K _T	-307	-119	2.5	1.4	0.1
Nanotube/Rod					
A ₆ K	-514	-173	2.5	1.5	0.6
A ₉ K	-727	-218	3.0	1.9	0.5

^aThe number of hydrogen bonds (per A_NK) between A_NK molecules. SS, AA, and AK refer to the hydrogen formed between peptide/peptide, alanine/alanine, and alanine/lysine, respectively.

water for each nanostructure. Here we can observe that intermolecular interaction, U_{inter} , is 3.6, 5.0, and 7.0 ($\times 10^4$ kJ mol $^{-1}$) for A₃K_C, A₆K, and A₉K, respectively. The largest portion of this interaction is of electrostatic nature, while only 8–14% is of van der Waals type. When considering the total potential energy, U_{total} , we can observe the same trend. Thus, in general, we note that the interaction energy between water and peptides increases with the peptide size, that is, the higher the peptide, the greater its stability of the corresponding nanostructure. This result is consistent with the experimental findings, where it was observed that tubular structures are much more stiff than lamellar ones.³⁵

Table 4 summarizes Coulomb (U_{Coul}) and van der Waals (U_{vdW}) contributions to the interaction energy between the

SLPs. Although the interaction energies are not solely responsible for membrane stabilization, they provide an estimate of the intensity of each type of peptide–peptide binding into the nanostructured system. Unlike lipid membranes and lipopeptide nanofibers, the electrostatic interactions dominate over the van der Waals interactions. Overall, we observe that both components increase with the peptide size. The electrostatic interaction constitutes 70–75% of total peptide attraction. A₃K_C is more stable than A₃K_T by 44 kJ/mol of peptides. Such an arrangement is most thermodynamically favorable. The prevalence of the U_{Coul} component was also observed for membranes involving other peptide classes.² In particular, the A₆K membrane has essentially the same U_{vdW} contribution, as the present nanotube structure. However, the U_{Coul} contribution for this nanotube is much smaller (100 kJ/mol of peptides) than that in the A₆K membrane.² Therefore, the A₆K peptides form tubular structures rather than bilayers. The A₉K nanorod exhibits the highest cohesive energy, 945 kJ mol $^{-1}$. All of these trends observed for the peptide–peptide interactions are consistent with that observed for peptide–water interactions.

In the previous work, we showed that peptides are well ordered if they are arranged in the form of membranes. In one direction, peptides are aligned to favor hydrogen bonding. In another direction, the ordering facilitates van der Waals interactions. To further explore the self-assembly, we calculated all hydrogen bonds formed between the peptides (Table 4, Figure 7) and between peptides and water (Figure 7, Table S2, Supporting Information). In addition, we decomposed the total number of hydrogen bonds to unveil individual contributions of each alanine (A) and lysine (K) residue. Each alanine residue has two polar groups (–CO proton acceptor and –NH proton donor). It can, in principle, form two peptide–peptide hydrogen bonds. The lysine residue, in turn, has a positively charged proton donor amino group. According to the terminations used in the synthesis of A_NK peptides, it also possesses two additional –NH and –CO groups. Therefore, the lysine moiety can form more than four peptide–peptide hydrogen bonds. The number of hydrogen bonds in the A₃K membranes is higher (Table 3), even though the number of amino acid residues is larger. This feature is due to bilayer organization, which optimizes direct contacts between the peptides. Four and a half hydrogen bonds (SS) per peptide were recorded in the A₃K_C membrane. Out of these bonds, 1.9 hydrogen bonds are formed between alanine residues (AA). A

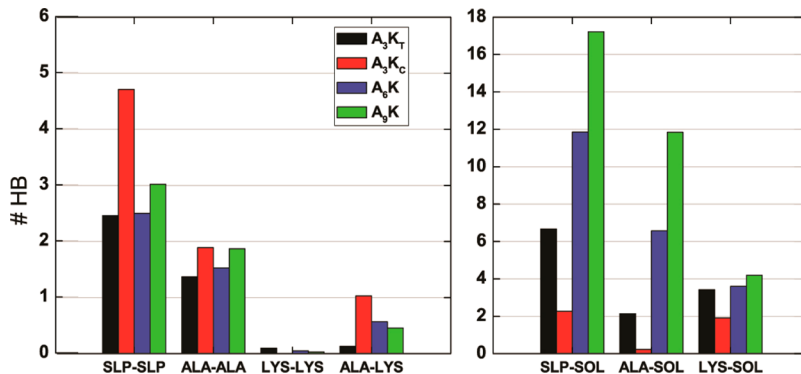


Figure 7. Number of hydrogen bonds between each pair of the A_nK systems and water. Protein is abbreviated as SLP, alanine residue is ALA, lysine residue is LYS, and water is SOL.

single (1.0) bond is formed between the alanine and lysine residues (AK). In the case of a nanorod, the total number of hydrogen bonds between A_9K peptides amounts to 2.5, whereas the decomposition by components provides 1.9 (AA) and 0.5 (AK). The AA bonds are formed between all alanine residues. Consequently, the number of hydrogen bonds is smaller for the alanine residues than for the lysine residues. Figure 7 depicts these numbers, in addition to peptide–water hydrogen bonds. The number of hydrogen bonds with water is, naturally, proportional to the size of the string, being 2.3 (A_3K_c membrane) and 17.2 (nanorod). Figures S1 and S2 (Supporting Information) show the orientation of hydrogen bonds in all systems. In the A_3K membranes, hydrogen bonds are arranged to enhance SLP packing. In the case of the A_6K nanotube, the hydrogen bonds arrange to preserve the tubular structure. Hydrogen bonding is responsible for the inner radius of the tube.

4. CONCLUSION

We employ atomistic molecular dynamics simulations to describe the structure and energetic properties of the selected nanostructures— A_3K membranes, A_6K nanotube, and A_9K nanorod. Our results confirm that the A_3K membranes are stable in two different configurations. The first configuration consists of SLPs tilted relative to the normal membrane plane (A_3K_c). The second configuration contains interdigitated SLPs (A_3K_T). Both membranes exhibit structure order at long separations. Consequently, these structures maintain the gel phase. A certain structure order of the A_6K peptides was recorded in cylindrical nanostructures. The long order is absent in the A_9K nanorod, though. We hypothesize that these structures exhibit properties of hydrogels, which are important in biotechnology.

The protein containing membranes are very thin, 2.6 (A_3K_c) and 1.9 nm (A_3K_T), as compared to lipid membranes. These values are consistent with the experiment. The A_6K nanotube exhibits an outer diameter of 4.9 nm, which is in excellent agreement with the experimental value, 5.0 ± 1.0 nm, from the AFM image. The diameter of the nanorod is 4.4 nm. Energy analysis, performed in terms of Coulomb and van der Waals contributions, shows that both components increase as the peptide size increases. The electrostatic interaction constitutes 70–75% of the total nonbonded potential energy. Nanotubular structures are clearly stable. The A_6K peptides form nanotubes, whereas the A_9K peptides form nanorods. Our results contribute to a better understanding of supramolecular structures obtained from surfactant-like peptides.

ASSOCIATED CONTENT

S Supporting Information

Additional technical information regarding MD simulations. This material is available free of charge via the Internet at <http://pubs.acs.org>.

AUTHOR INFORMATION

Corresponding Author

*E-mail: fileti@unifesp.br, fileti@gmail.com. Phone: +55 12 3309-9573. Fax: +55 12 3921-8857.

Notes

The authors declare no competing financial interest.

ACKNOWLEDGMENTS

This work was supported by grants from Brazilian agencies FAPESP and CNPq. We thank Dr. Vitaly Chaban for his critical review and comments.

REFERENCES

- (1) Souza, M. I.; Jaques, Y. M.; de Andrade, G. P.; Ribeiro, A. O.; da Silva, E. R.; Fileti, E. E.; Avilla Ede, S.; Pinheiro, M. V.; Krambrock, K.; Alves, W. A. Structural and photophysical properties of peptide micro/nanotubes functionalized with hypericin. *J. Phys. Chem. B* **2013**, *117* (9), 2605–2614.
- (2) Colherinhos, G.; Fileti, E. Molecular Description of Surfactant-like Peptide Based Membranes. *J. Phys. Chem. C* **2014**, *118* (18), 9598–9603.
- (3) Dehsorkhi, A.; Castelletto, V.; Hamley, I. W. Self-assembling amphiphilic peptides. *J. Pept. Sci.* **2014**, *20*, 453–467.
- (4) Caruso, M.; Placidi, E.; Gatto, E.; Mazzuca, C.; Stella, L.; Bocchinfuso, G.; Palleschi, A.; Formaggio, F.; Toniolo, C.; Venanzi, M. Fibrils or globules? Tuning the morphology of peptide aggregates from helical building blocks. *J. Phys. Chem. B* **2013**, *117* (18), 5448–5459.
- (5) Lemkul, J. A.; Bevan, D. R. Aggregation of Alzheimer's amyloid beta-peptide in biological membranes: a molecular dynamics study. *Biochemistry* **2013**, *52* (29), 4971–4980.
- (6) Munoz, E.; Sreelatha, A.; Garriga, R.; Baughman, R. H.; Goux, W. J. Amyloidogenic peptide/single-walled carbon nanotube composites based on tau-protein-related peptides derived from AcPHF6: preparation and dispersive properties. *J. Phys. Chem. B* **2013**, *117* (25), 7593–7604.
- (7) Hosseinkhani, H.; Hong, P.-D.; Yu, D.-S. Self-Assembled Proteins and Peptides for Regenerative Medicine. *Chem. Rev.* **2013**, *113*, 4837–4861.
- (8) Mazza, M.; Notman, R.; Anwar, J.; Rodger, A.; Hicks, M.; Parkinson, G.; McCarthy, D.; Daviter, T.; Moger, J.; Garrett, N.; Mead, T.; Briggs, M.; Schätzlein, A. G.; Uchegbu, I. F. Nanofiber-Based Delivery of Therapeutic Peptides to the Brain. *ACS Nano* **2013**, *7*, 1016–1026.

- (9) Lemkul, J. A.; Bevan, D. R. The role of molecular simulations in the development of inhibitors of amyloid beta-peptide aggregation for the treatment of Alzheimer's disease. *ACS Chem. Neurosci.* **2012**, *3* (11), 845–856.
- (10) Zhang, P.; Cheetham, A. G.; Lin, Y.-A.; Cui, H. Self-Assembled Tat Nanofibers as Effective Drug Carrier and Transporter. *ACS Nano* **2013**, *7*, 5965–5977.
- (11) Yu, T.; Schatz, G. C. Free energy profile and mechanism of self-assembly of peptide amphiphiles based on a collective assembly coordinate. *J. Phys. Chem. B* **2013**, *117* (30), 9004–9013.
- (12) Hamley, I. W. Self-assembly of amphiphilic peptides. *Soft Matter* **2011**, *7*, 4122–4138.
- (13) Quadir, M. A.; Martin, M.; Hammond, P. T. Clickable Synthetic Polypeptides—Routes to New Highly Adaptive Biomaterials. *Chem. Mater.* **2014**, *26*, 461–476.
- (14) Li, Y.; Shao, M.; Zheng, X.; Kong, W.; Zhang, J.; Gong, M. Self-Assembling Peptides Improve the Stability of Glucagon-like Peptide-1 by Forming a Stable and Sustained Complex. *Mol. Pharmaceutics* **2013**, *10*, 3356–3365.
- (15) Schlamadinger, D. E.; Wang, Y.; McCammon, J. A.; Kim, J. E. Spectroscopic and computational study of melittin, cecropin A, and the hybrid peptide CM15. *J. Phys. Chem. B* **2012**, *116* (35), 10600–10608.
- (16) Nichols, M.; Kuljanin, M.; Nategholeslam, M.; Hoang, T.; Vafaei, S.; Tomberli, B.; Gray, C. G.; DeBruin, L.; Jelokhani-Niaraki, M. Dynamic turn conformation of a short tryptophan-rich cationic antimicrobial peptide and its interaction with phospholipid membranes. *J. Phys. Chem. B* **2013**, *117* (47), 14697–14708.
- (17) Nicolas, P.; Mor, A. Peptides as weapons against microorganisms in the chemical defense system of vertebrates. *Annu. Rev. Microbiol.* **1995**, *49*, 277–304.
- (18) Javadpour, M. M.; Barkley, M. D. Self-assembly of designed antimicrobial peptides in solution and micelles. *Biochemistry* **1997**, *36* (31), 9540–9549.
- (19) Zhang, L.; Vidu, R.; Waring, A. J.; Lehrer, R. I.; Longo, M. L.; Stroeven, P. Electrochemical and Surface Properties of Solid-Supported, Mobile Phospholipid Bilayers on a Polyion/Aalkylthiol Layer Pair Used for Detection of Antimicrobial Peptide Insertion. *Langmuir* **2002**, *18* (4), 1318–1331.
- (20) Schmitt, M. A.; Weisblum, B.; Gellman, S. H. Unexpected relationships between structure and function in alpha,beta-peptides: antimicrobial foldamers with heterogeneous backbones. *J. Am. Chem. Soc.* **2004**, *126* (22), 6848–6849.
- (21) Chen, C.; Pan, F.; Zhang, S.; Hu, J.; Cao, M.; Wang, J.; Xu, H.; Zhao, X.; Lu, J. R. *Biomacromolecules* **2010**, *11*, 402–411.
- (22) Mishra, A.; Lai, G. H.; Schmidt, N. W.; Sun, V. Z.; Rodriguez, A. R.; Tong, R.; Tang, L.; Cheng, J.; Deming, T. J.; Kamei, D. T.; Wong, G. C. Translocation of HIV TAT peptide and analogues induced by multiplexed membrane and cytoskeletal interactions. *Proc. Natl. Acad. Sci. U. S. A.* **2011**, *108* (41), 16883–16888.
- (23) Lind, T. K.; Zielinska, P.; Wacklin, H. P.; Urbanczyk-Lipkowska, Z.; Cardenas, M. Continuous flow atomic force microscopy imaging reveals fluidity and time-dependent interactions of antimicrobial dendrimer with model lipid membranes. *ACS Nano* **2014**, *8* (1), 396–408.
- (24) Gao, B.; Zhu, S. An insect defensin-derived beta-hairpin peptide with enhanced antibacterial activity. *ACS Chem. Biol.* **2014**, *9* (2), 405–413.
- (25) Etayash, H.; Norman, L.; Thundat, T.; Kaur, K. Peptide-bacteria interactions using engineered surface-immobilized peptides from class IIa bacteriocins. *Langmuir* **2013**, *29* (12), 4048–4056.
- (26) Xia, H.; Gu, G.; Hu, Q.; Liu, Z.; Jiang, M.; Kang, T.; Miao, D.; Song, Q.; Yao, L.; Tu, Y.; Chen, H.; Gao, X.; Chen, J. Activatable cell penetrating peptide-conjugated nanoparticles with enhanced permeability for site-specific targeting delivery of anticancer drug. *Bioconjugate Chem.* **2013**, *24* (3), 419–430.
- (27) Zhang, P.; Cheetham, A.; Lin, Y.-A.; Cui, H. Self-assembled Tat nanofibers as effective drug carrier and transporter. *ACS Nano* **2013**, *7* (7), 5965–5977.
- (28) Palffy, R.; Gardlik, R.; Behuliak, M.; Kadasi, L.; Turna, J.; Celec, P. On the physiology and pathophysiology of antimicrobial peptides. *Mol. Med.* **2009**, *15* (1–2), 51–59.
- (29) Gottler, L. M.; Ramamoorthy, A. Structure, membrane orientation, mechanism, and function of pexiganan—a highly potent antimicrobial peptide designed from magainin. *Biochim. Biophys. Acta* **2009**, *1788* (8), 1680–1686.
- (30) He, C.; Han, Y.; Zhu, L.; Deng, M.; Wang, Y. Modulation of Abeta(1–40) peptide fibrillar architectures by Abeta-based peptide amphiphiles. *J. Phys. Chem. B* **2013**, *117* (36), 10475–10483.
- (31) Xu, H.; Wang, Y.; Ge, X.; Han, S.; Wang, S.; Zhou, P.; Shan, H.; Zhao, X.; Lu, J. R. Twisted Nanotubes Formed from Ultrashort Amphiphilic Peptide I₃K and Their Templating for the Fabrication of Silica Nanotubes. *Chem. Mater.* **2010**, *22*, 5165–5173.
- (32) Dehsorkhi, A.; Castelletto, V.; Hamley, I. W.; Seitsonen, J.; Ruokolainen, J. Interaction between a Cationic Surfactant-like Peptide and Lipid Vesicles and Its Relationship to Antimicrobial Activity. *Langmuir* **2013**, *29*, 14246–14253.
- (33) Zhang, S. Lipid-like Self-Assembling Peptides. *Acc. Chem. Res.* **2012**, *45* (12), 2142–2150.
- (34) Zhao, X.; Pan, F.; Xu, H.; Yaseen, M.; Shan, H.; Hauser, C. A.; Zhang, S.; Lu, J. R. Molecular self-assembly and applications of designer peptide amphiphiles. *Chem. Soc. Rev.* **2010**, *39* (9), 3480–3498.
- (35) Xu, H.; Wang, J.; Han, S.; Wang, J.; Yu, D.; Zhang, H.; Xia, D.; Zhao, X.; Waigh, T. A.; Lu, J. R. Hydrophobic-Region-Induced Transitions in Self-Assembled Peptide Nanostructures. *Langmuir* **2009**, *25* (7), 4115–4123.
- (36) Best, R. B.; Zhu, X.; Shim, J.; Lopes, P. E.; Mittal, J.; Feig, M.; Mackerell, A. D., Jr. Optimization of the additive CHARMM all-atom protein force field targeting improved sampling of the backbone phi, psi and side-chain chi(1) and chi(2) dihedral angles. *J. Chem. Theory Comput.* **2012**, *8* (9), 3257–3273.
- (37) Parrinello, M.; Rahman, A. Polymorphic transitions in single crystals: A new molecular dynamics method. *J. Appl. Phys.* **1981**, *52*, 7182–7192.
- (38) Hess, B.; Bekker, H.; Berendsen, H. J. C.; Fraaije, J. G. E. M. LINCS: A linear constraint solver for molecular simulations. *J. Comput. Chem.* **1997**, *18*, 1463.
- (39) Darden, T.; York, D.; Pedersen, L. Particle mesh Ewald: An N-log(N) method for Ewald sums in large systems. *J. Chem. Phys.* **1993**, *98*, 10089–10099.
- (40) Lindahl, E.; Hess, B.; van der Spoel, D. GROMACS 3.0: a package for molecular simulation and trajectory analysis. *J. Mol. Model.* **2001**, *7*, 306–317.
- (41) Berendsen, H. J. C.; van der Spoel, D.; van Drunen, R. GROMACS - A message-passing parallel molecular-dynamics implementation. *Comput. Phys. Commun.* **1995**, *91*, 43–56.
- (42) Humphrey, W.; Dalke, A.; Schulter, K. VMD: visual molecular dynamics. *J. Mol. Graphics* **1996**, *14* (1), 33-8, 27-8.
- (43) Yu, T.; Lee, O.-S.; Schatz, G. C. Steered molecular dynamics studies of the potential of mean force for peptide amphiphile self-assembly into cylindrical nanofibers. *J. Phys. Chem. A* **2013**, *117* (32), 7453–7460.
- (44) Lee, O.-S.; Stupp, S. I.; Schatz, G. C. Atomistic molecular dynamics simulations of peptide amphiphile self-assembly into cylindrical nanofibers. *J. Am. Chem. Soc.* **2011**, *133* (10), 3677–3683.
- (45) Yang, H.; Tyagi, P.; Kadam, R. S.; Holden, C. A.; Kompella, U. B. Hybrid dendrimer hydrogel/PLGA nanoparticle platform sustains drug delivery for one week and antiglaucoma effects for four days following one-time topical administration. *ACS Nano* **2012**, *6* (9), 7595–7606.
- (46) Allen, W. J.; Lemkul, J. A.; Bevan, D. R. GridMAT-MD: a grid-based membrane analysis tool for use with molecular dynamics. *J. Comput. Chem.* **2009**, *30* (12), 1952–1958.